CrossMark

TECHNICAL PAPER

A MEMS piezoelectric solid disk gyroscope with improved sensitivity

**Yuxiang Cheng · Weiping Zhang · Jian Tang ·
Dianjun Sun · Wenyuan Chen**

Abstract This paper introduces a MEMS piezoelectric solid disk gyroscope. The gyroscope operates in an in-plane elliptic bulk acoustic wave mode with a frequency of 284 kHz. This gyroscope is an improvement of the solid piezoelectric gyroscope. A device, 6 mm in diameter, has been fabricated through the microelectromechanical systems process, and achieved a relatively high sensitivity and bias instability. In this paper, it is described that the design, fabrication, circuit system and characteristics of the piezoelectric solid disk gyroscope.

1 Introduction

The micromachined gyroscopes have attracted a lot of attention in these years, for their small size, low cost, and high sensitivity all the time. Most of these MEMS gyroscopes need to be employed by electrostatic, or electromagnetic, or piezoelectric mechanisms for driving and sensing (Liu et al. 2009). In most reports, piezoelectric gyroscopes deployed composite layers of the piezoelectric film, silicon and metal electrodes based on a cantilever structure as the power transducer rather than the resonator, which decreases the energy conversion efficiency and increases the energy loss. In 2006, Maenaka and Kohara proposed a solid micro piezoelectric gyroscope (Maenaka et al. 2006), which only used a prism-shaped bulk-PZT with some electrodes on its

Y. Cheng · W. Zhang (✉) · J. Tang · D. Sun · W. Chen
National Key Laboratory of Science and Technology on Micro/
Nano Fabrication Laboratory, Laboratory for Thin Film
and Micro Fabrication of the Ministry of Education, Department
of Micro-Nano Electronics, School of Electronic Information
and Electrical Engineering, Shanghai Jiao Tong University,
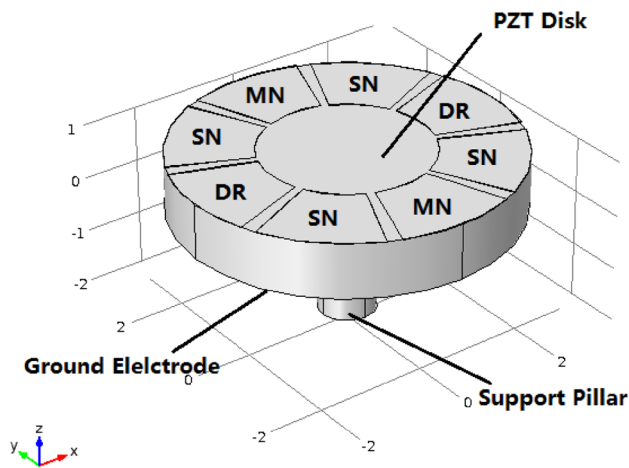Shanghai 200240, China
e-mail: zhangwp@sjtu.edu.cn

surface. This design deployed a bulk piezoelectric structure as an entire resonator without any other elastic structures, to increase the shock resistance, the energy conversion efficiency and decrease the fabrication complexity. However, the PZT material itself has the characteristic of low quality factor, low output signal and much mechanical noise, compared with the silica-based material. As a result, how to increase the output signal and the sensitivity is a hot topic for piezoelectric gyroscopes (Cheng et al. 2013).

On the other hand, the development of the MEMS silicon vibrating gyroscopes shows that the mode matching is a valid solution to increase the output signal and sensitivity of the gyroscopes (Tanaka et al. 1995). The mode matching is to match the resonant frequency between the drive mode and the sense mode, and to eliminate the frequency split. In most of the vibrating gyroscopes, the exact calculation and design should be made to implement a good characteristic. The ring vibrating gyroscope is a kind of degenerate gyroscope (He and Najafi 2002), which has an inherent axial symmetric resonator and utilizes a degenerate vibration mode pair as the drive and sense modes to maximize the energy transfer between the two modes. The degenerate gyroscopes have an inherent mode matching, which improves the characteristic and increases the sensitivity of the devices. In recent years, more and more attentions have been attracted by the degenerate gyroscopes, including the ring vibrating gyroscopes (He and Najafi 2002; Ayazi and Najafi 2000, 2001) and the hemispherical resonator gyroscopes (Zotov et al. 2012; Pai et al. 2012; Cho et al. 2013).

This paper proposes a novel disk-like solid piezoelectric gyroscope based on the in-plane bulk acoustic wave (BAW) resonance. This design combines the solid piezoelectric gyroscopes with a disk-like resonant structure which is inherently mode matched. The structure not only obtains the high shock resistance and energy conversion efficiency

Fig. 1 Schematic diagram of the MEMS BAW piezoelectric gyroscope

of the solid gyroscopes, but also decreases the frequency split by an inherent mode matched structure, which results in improving the output and sensitivity of the device.

2 Operation and design

Figure 1 shows a schematic view of the center-supported BAW piezoelectric gyroscope. The resonator of 6 mm in diameter and 1 mm in thickness is made from a PZT-42 wafer which is polarized along z axis, whose both sides are covered with metal electrodes. There are three kinds of electrodes on the front side: drive (DR), sense (SN) and monitor (MN) electrode, which are 45° apart each other to minimize excessive frequency split between the drive and sense modes. The back surface is a whole electrode (ground electrode). A support pillar is fixed on the resonator at the center of the back side.

With origin set at the center of the disk, the plane polar coordinates r and θ are used in this paper. The two drive electrodes are placed at $\theta = 0°$ and 180° along the x axis. In order to excite the device into resonance, two identical AC drive voltage signals are applied to the two drive electrodes. The disk-like gyroscope vibrates in the in-plane elliptical mode, which involves both radial and circumferential displacements in the disk. The sense electric current signals are detected from the sense electrodes, located at $\theta = 45°$, 135°, 225° and 315°. The monitor electrodes at $\theta = 90°$ and 270° are used as the real-time monitor to trace the resonant frequency and amplitude of the device, and form a feedback control system. The finite element method modal analysis shows a degenerate in-plane mode for this piezoelectric disk gyroscope. The result shows a pair of modes with the frequency of about 280.5 kHz and a quite
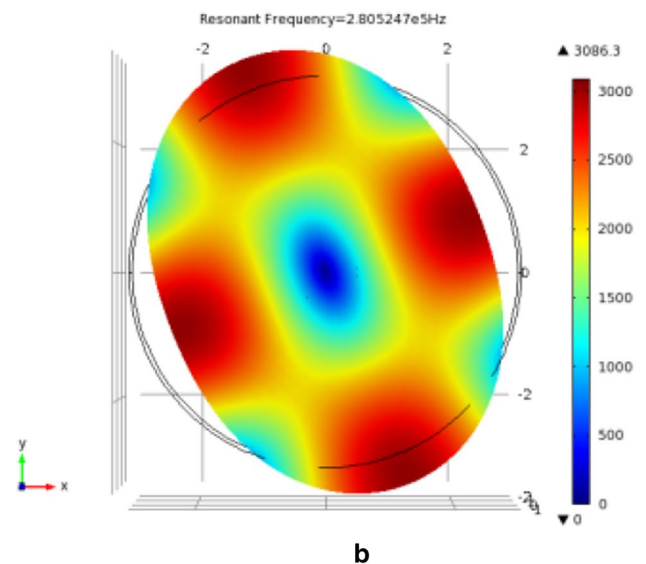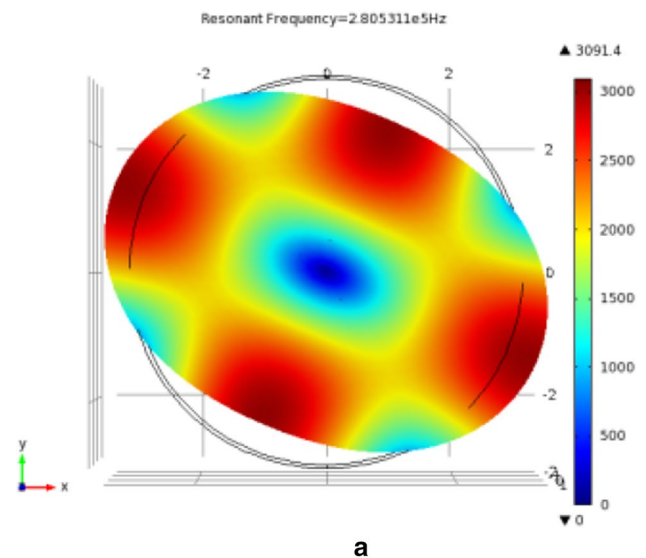

Fig. 2 Elliptic mode from the modal analysis results, BAW in-plane degenerate mode. **a** Drive mode; **b** sense mode

small frequency split (<7 Hz), as shown in Fig. 2. These degenerate modes are named elliptic modes, or flexural modes, which have the identical resonant frequency, and the resonant directions are spatially 45° apart. According to the 2-D elastic theory governing the in-plane vibrations of a disk, the radial (U) and circumferential (V) components of the displacement vector (u) at the drive mode, respectively, could be expressed in the following formula (Hao et al. 2004):

$$U = \left[A\frac{d}{d_r} J_2\left(\omega\frac{r}{\alpha}\right) + \frac{2}{r}AJ_2\left(\omega\frac{r}{\beta}\right) \right]\cos(2\theta) \tag{1a}$$

$$V = -\left[B\frac{d}{d_r} J_2\left(\omega\frac{r}{\beta}\right) + \frac{2}{r}AJ_2\left(\omega\frac{r}{\alpha}\right) \right]\sin(2\theta) \tag{1b}$$
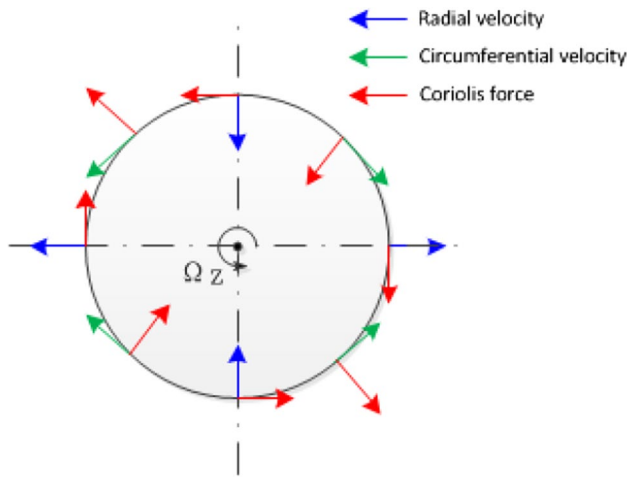
Fig. 3 The motion analysis of the BAW disk gyroscope

where A, and B are the constants of the elastic waves, in the unit of squared meter. J_2 is the Bessel functions of the first kind. Both α, β are only decided by the material parameters. ω is the resonant frequency of the device. And the displacement at the sense mode is similar with (1), except that the sinusoidal and cosine items are exchanged.

Figure 3 shows the motion analysis of the gyroscope. Excited an AC drive signal on the drive electrodes, the gyroscope will oscillate at the drive mode as shown in Fig. 2a. According to (1), the maximum radial velocity happens at $\theta = 0°$, 90°, 180°, and 270°, and does not happen at $\theta = 45°$, 135°, 225°, and 315°. On the other hand, the max circumferential velocity happens at $\theta = 45°$, 135°, 225°, and 315°, and does not happen at $\theta = 0°$, 90°, 180°,

and 270°. Based on the Coriolis effect, the Coriolis force can be expressed as,
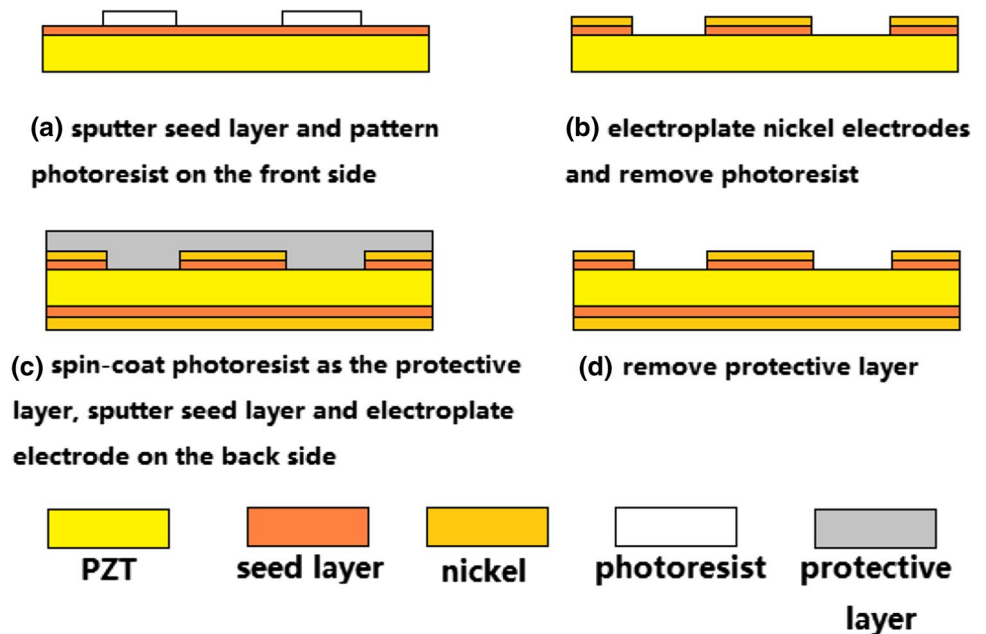
$$F_c = 2\mu \times \Omega_z \tag{2}$$

Under the Coriolis effect, when an angular rate along the z axis (Ω_z) is inputted, the oscillation will transfer into the sense mode, as shown in Fig. 2b. The resonant amplitude of the sense mode depends on the amplitude of the drive mode and the inputted angular rate. Thus, the inputted angular rate can be measured by the sense electrodes. The output signal is proportional to the inputted angular rate.

3 Fabrication

The BAW piezoelectric gyroscopes are fabricated on 1 mm thick PZT-42 wafers by an extremely simple fabrication process. The basic outline of the process is shown in Fig. 4. The fabrication starts from sputtering the Cr/Cu seed layer on the front side of wafer and patterning photoresist on the seed layer. Then a 5 μm thick Ni layer is electroplated as the electrodes, and a 10 μm thick photoresist is spin-coated on the front side as a protective layer. Next, the ground electrode is electroplated after a seed layer is sputtered on the back side of the wafer. Finally, the protective layer on the front side is removed in acetone and alcohol.

After MEMS fabrication process, wafer is cut into a 6-mm-diameter disk by using laser cutting. Then the PZT disk is glued on the support pillar after center-aligning with a special clamp. Figure 5 shows the piezoelectric disk and the fixed gyroscopes on the PCB.

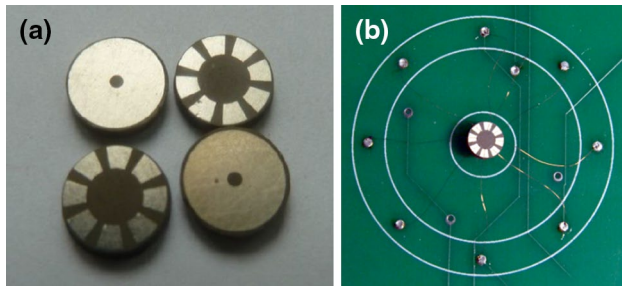**Fig. 4** The process flow of piezoelectric disk on PZT wafer

(a) sputter seed layer and pattern photoresist on the front side

(b) electroplate nickel electrodes and remove photoresist

(c) spin-coat photoresist as the protective layer, sputter seed layer and electroplate electrode on the back side

(d) remove protective layer

PZT   seed layer   nickel   photoresist   protective layer

Fig. 5 Photograph of **a** piezoelectric disk, **b** fixed gyroscope on the PCB

4 Circuit architecture

Figure 6 shows the block diagram of the implemented high frequency piezoelectric gyroscope system. The system requires three basic blocks: the drive block to actuate the gyroscope at the resonance frequency, the sense block with demodulator to extract the angular rate and monitor closed-loop block to track the motion of the gyroscope.

Applied two same AC drive voltages (U_d) on the drive electrodes at $\theta = 0°$ and $180°$, the device oscillates at the drive mode.

$$U_d = A_d \cos \omega t \tag{3}$$

The signal (U_m) on the monitor electrode at $\theta = 90°$ is sensed by a charge amplifier,

$$U_m = A_m \cos(\omega t + \pi) \tag{4}$$

and extracts the amplitude signal (A_m) and frequency signal (ω), which are inputted into phase locked loop (PLL) and auto gain control (AGC) modules, respectively. PLL is designed to track and lock the resonance frequency of the device in real time. And AGC is designed to keep the drive voltage stable. U_m and U_d have the same frequency and a signal difference of $180°$. Finally, the signals are feed backed to the drive loop, which ensures that the drive signals track the working status of the gyroscope in real time.
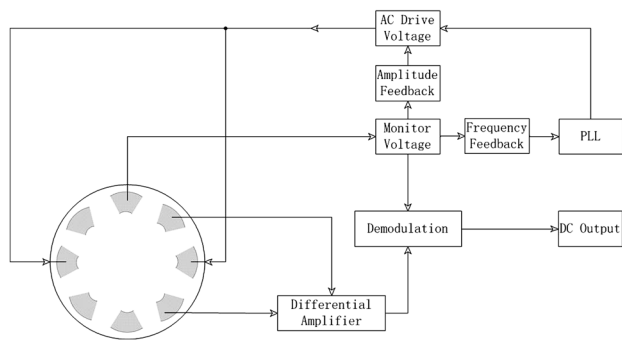

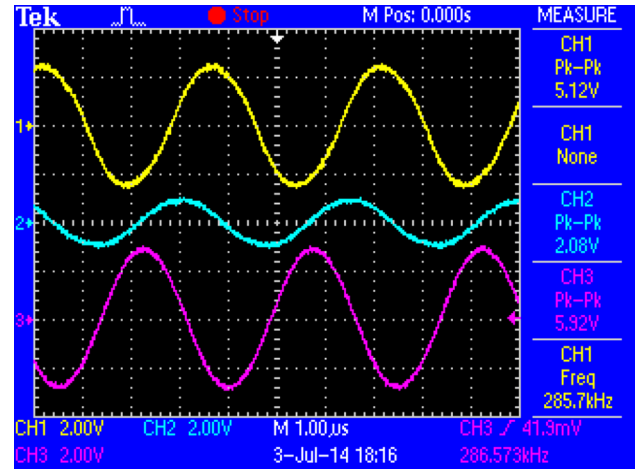**Fig. 6** System block diagram

Fig. 7 The working status of the gyroscopes: drive, sense, and monitor signals

Differential amplifier in the detect part is designed to get the difference of two adjacent sense electrodes signal (U_s) and eliminate interfere noises.

$$U_s = 2A_s \sin \omega t \tag{5}$$

U_s has the same frequency with U_d, and has a phase difference of $90°$. Demodulator will multiply the differential signal and the reference signal which is the phase shifted signal from the monitor loop, and get the low frequency signal that will reflect the gyroscope rotation angular directly

$$U_{demo} = U_{ref} \times U_s == A_m A_s (1 - \cos 2\omega t) \tag{6}$$

$$V_{out} = A_m A_s \tag{7}$$

In condition of none angular rate inputted, V_{out} is the zero rate output (ZRO) of the gyroscope.

As shown in Fig. 7, channel 1, 2 and 3 reflect the signals on the drive, sense and monitor electrodes, respectively, in condition of none angular rate inputted. It is shown that: (a) drive and monitor signals have the almost same amplitude and opposite phase; (b) sense signal have smaller amplitude than drive signal, and a phase difference of about $90°$; (c) the device operates at the frequency of 286 kHz; (d) according to (7), the ZRO of the gyroscope is around 3 V, which is caused by the electronic charge coupling on the electrodes. These conclusions could well agree with the theoretical analysis result shown above. Actuated by a 5 V drive voltage, the sense voltage after the charge amplifier is about 2 V.

Eliminating the influence of the ZRO, the output signal V_{out} could reflect the inputted angular rate directly. Figure 8 shows the final output signal with a sinusoidal angular rate input.
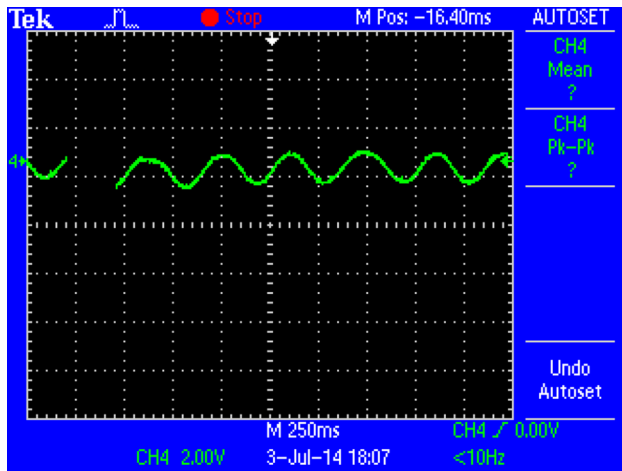
Fig. 8 Output signal with a sinusoidal angular rate input

Fixed the circuit board on the rotary table, the whole gyroscope system is shown in Fig. 9. By controlling the rotary table, the sensitivity of the gyroscope could be measured. The measurement results will be listed in next sections.

Fig. 9 The whole gyroscope system with a rotary table, and the PCB circuit

5 Measurement results

Mode testing of the gyroscope is performed to validate the sensor's vibration mode without any tuning method. The harmonic response is tested by a PV70A impedance analyser in air. A sinusoidal drive signal is applied to the drive electrode with a sweep frequency from 270 to 300 kHz. Figure 10 shows the measured frequency response of the drive mode in air, exhibiting a quality factor of 402 at a frequency of 285.6 kHz. The test is performed repeatedly on different electrodes of the same device, and the result shows a frequency split of less than 30 Hz. This result could match the simulation result (a frequency of 280.5 kHz) properly.

The vibration mode is tested by Politec-300 scanning vibrometer. Excited by a 5 V sinusoidal drive voltage, the response curves of the radial and axial displacement is shown in Fig. 11. It is shown that the gyroscope resonates at a frequency of 284 kHz at the in-plane mode, and at a frequency of 335 kHz at the out-of-plane mode (as shown in Fig. 12). The resonant frequency tested by vibrometer has a little of difference with the mode testing, as the impendence of the PCB is also taken into account. In consideration of the practical situation, the results from vibrometer are more consistent than the impendence analyzer. The maximum radial displacement of the gyroscope is about 45 pm at the elliptic mode.
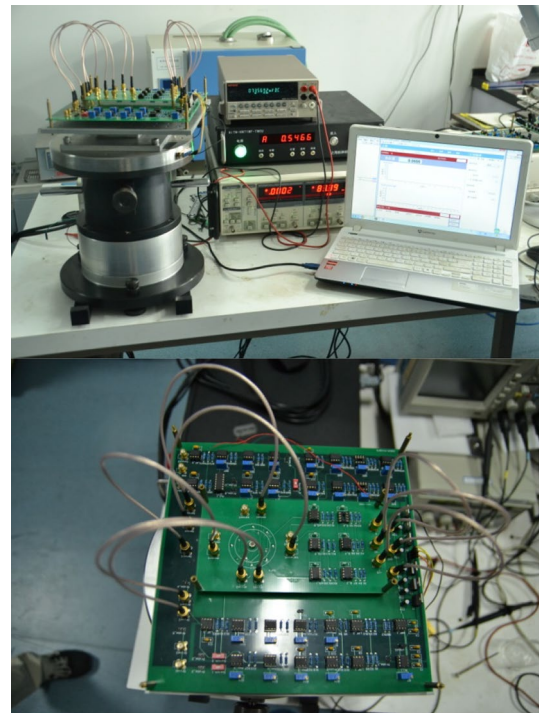
The sensor's output voltage is measured at different angular rates. The gyroscope has an angular rate sensitivity of about 340 µV/°/s and remains linear with applied rotation rate as high as 500°/s, as shown in Fig. 13. The zero rate output of the gyroscope is sampled over a period of more than 24 h at room temperature and pressure. Using the collected ZRO data, an Allan variance analysis was performed to characterize the long-term stability of the mode matching device. The measured bias instability of the gyroscope is 10.1°/s on average, while the best observed result is less than 1°/s.

6 Discussion

The design specifications and measurement results of the 6-mm-diameter BAW piezoelectric gyroscope are summarized in Table 1. The measured results could match the simulation properly. Although the Q factor is only about 400, the frequency split is quite small, which means that the Q factor is not mainly effected by the disk structure but by the material itself. In consideration of the quality factor of the PZT-42 material, the Q factor of the gyroscope is acceptable. However, the rate sensitivity and the bias instability of the current gyroscope are much better than that of the solid piezoelectric gyroscope previously reported (Maekawa et al. 2010). In addition to these changes, the
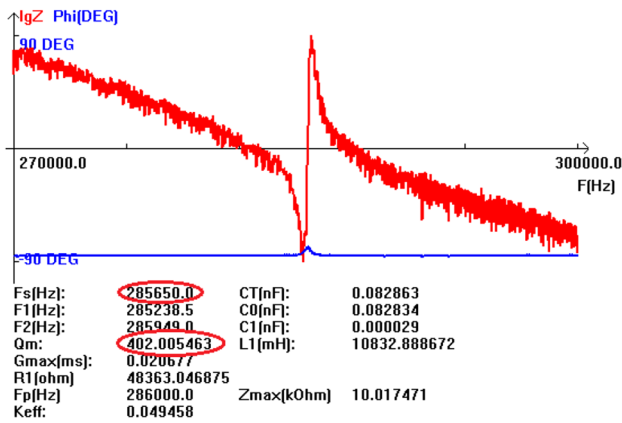
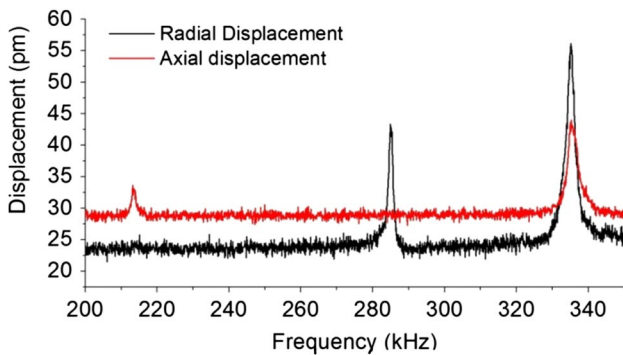**Fig. 10** The frequency response curve of the drive mode

Fig. 11 The response curves of the radial and axial displacements
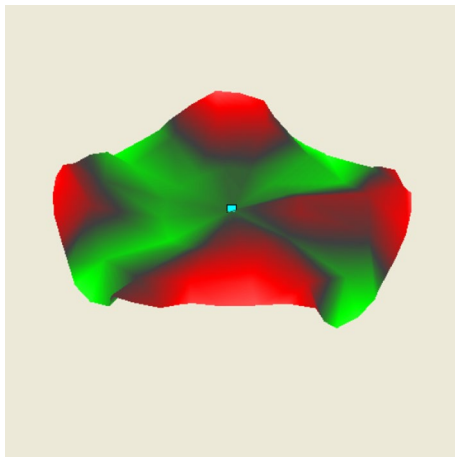

Fig. 12 Displacement nephogram of vibration test at an out-of-plane mode with a frequency of 335 kHz

reference noise inputted by the interface electronics can be reduced by interfacing the device with an application specific integrated circuit (ASIC), and the characteristic would be better.
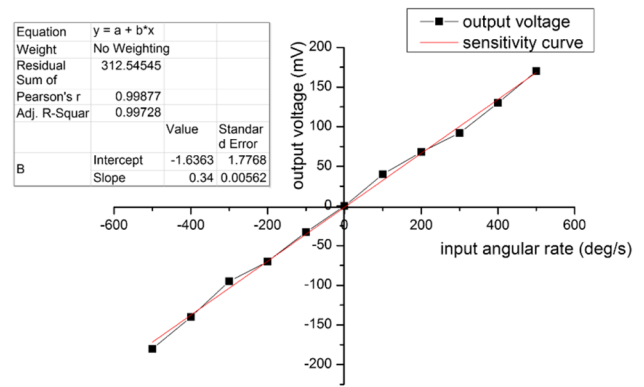

Fig. 13 The measured rate sensitivity results of the gyroscope

Table 1 Summary of design specifications for the BAW piezoelectric gyroscope

Device parameter	Value
Size in diameter	6 mm
Operation frequency	280.5 kHz (simulation) 284 kHz (measured)
Frequency split	<30 Hz
Q factor	402
Rate sensitivity	340 µV/°/s
Dynamic range	>500°/s
Bias instability	10.1°/s (average) 1°/s (best)

7 Conclusion

A 6-mm-diameter BAW solid piezoelectric gyroscope is designed and fabricated on the PZT-42 wafer by a relatively simple fabrication process. The device provides a Q factor of 402 and a small frequency split of less than 30 Hz, with an operation frequency of 284 kHz. The gyroscope remains a good linearity at applied rotation rate as high as 500°/s, with a sensitivity of 340 µV/°/s. The measured bias instability of the gyroscope is 10.1°/s on average.

References

Ayazi F, Najafi K (2000) High aspect-ratio combined poly and single-crystal silicon (HARPSS) MEMS technology. J Microelectromech Syst 9(3):288–294

Ayazi F, Najafi K (2001) A HARPSS polysilicon vibrating ring gyroscope. J Microelectromech Syst 10(2):169–179

Cheng YX, Zhang WP et al (2013) MEMS-based piezoelectric BAW resonator based on out-of-plane degenerate mode for micro angular detector. Electron Lett 49(6):406–407

Cho J, Woo JK, Yan J et al (2013) A high-Q birdbath resonator gyroscope (BRG). In: transducers and eurosensors XXVII: the 17th international conference on solid-state sensors, actuators and microsystems (TRANSDUCERS and EUROSENSORS XXVII). IEEE Press, New York, pp 1847–1850

Hao Z, Pourkamali S, Ayazi F (2004) VHF single-crystal silicon elliptic bulk-mode capacitive disk resonators-part I: design and modeling. J Microelectromech Syst 13(6):1043–1053

He G, Najafi K (2002) A single-crystal silicon vibrating ring gyroscope. In: The fifteenth IEEE international conference on IEEE micro electro mechanical systems, pp 718–721

Liu K, Zhang W, Chen W et al (2009) The development of micro-gyroscope technology. J Micromech Microeng 19(11):113001

Maekawa K, Tanaka Y, Fujita T, Maenaka K (2010) Proposal of 2-axis bulk-PZT gyroscope. Serv Robot Mechatron 15:305–308

Maenaka K et al (2006) Novel solid micro-gyroscope Micro Electro Mechanical Systems, MEMS 2006, Istanbul, pp 634–637

Pai P, Chowdhury FK, Mastrangelo CH et al (2012) MEMS-based hemispherical resonator gyroscopes Sensors, 2012 IEEE. IEEE Press, New York, pp 1–4

Tanaka K, Mochida Y, Sugimoto M et al (1995) A micromachined vibrating gyroscope. Sens Actuators A Phys 50(1):111–115

Zotov SA, Trusov AA, Shkel AM (2012) Three-dimensional spherical shell resonator gyroscope fabricated using wafer-scale glassblowing. J Microelectromech Syst 21(3):509–510